Preliminary investigation of thermal behaviour of PCM based latent heat thermal energy storage

Octavian G. Pop[1], *Lucian* Fechete Tutunaru[2], *Florin* Bode[1] and *Mugur C.* Balan[1,*]

[1]Technical University of Cluj-Napoca, Dept. of Mechanical Engineering, Bd. Muncii 103-105, 400641, Cluj-Napoca, Romania
[2]Technical University of Cluj-Napoca, Dept. of Automotive Engineering and Transports, Bd. Muncii 103-105, 400641, Cluj-Napoca, Romania

Abstract. Solid-liquid phase change is used to accumulate and release cold in latent heat thermal energy storage (**LHTES**) in order to reduce energy consumption of air cooling system in buildings. The storing capacity of the **LHTES** depends greatly on the exterior air temperatures during the summer nights. One approach in intensifying heat transfer is by increasing the air's velocity. A **LHTES** was designed to be integrated in the air cooling system of a building located in Bucharest, during the month of July. This study presents a numerical investigation concerning the impact of air inlet temperatures and air velocity on the formation of solid **PCM**, on the cold storing capacity and energy consumption of the **LHTES**. The peak amount of accumulated cold is reached at different air velocities depending on air inlet temperature. For inlet temperatures of 14°C and 15°C, an increase of air velocity above 50% will not lead to higher amounts of cold being stored. For Bucharest during the hottest night of the year, a 100 % increase in air velocity will result in 5.02% more cold being stored, at an increase in electrical energy consumption of 25.30%, when compared to the reference values.

1 Introduction

Worldwide effort is being dedicated to the reduction of energy consumption in the buildings sector, as about 40% of the global energy consumption is used in buildings [1]. The energy efficiency of air cooling systems can be enhanced by storing the cold available during summer nights in latent heat thermal energy storage systems (**LHTES**). These technologies use phase change materials (**PCM**), and their capability of enhancing the energy efficiency of fresh air conditioning systems have been the subject of many reviews [2-8].

Cooling applications using **PCM** are still in a phase where demonstration and research is required [8]. Considering that, the solidification process takes place due to the low ambient temperatures during the night the selection of the appropriate **PCM** plays a very important role. In [6] thermo-physical properties that the **PCM** must poses are presented. In [9] a selection algorithm is presented that takes into account the climatic parameters.

Organic **PCM** such as paraffin waxes are available on the market [10, 11].

Paraffin waxes are known to have a range of temperatures in which phase change occurs, and their thermo-physical properties and thermal behaviour of commercially available paraffin during solidification and melting are studied in [12-16]. Modern colorimetric techniques are necessary in order to accurately determine the variation of the heat flux with temperature during phase change. Once this variation is known, the specific heat, or apparent heat capacity variation with temperature, of the **PCM** can be determined, through thermal balance equations [12, 13].

For accumulation of maximum amount of cold, both the air inlet temperature and the air velocity present a high influence [17]. It was found that for the same flow rate and solidification time, with inlet air temperatures of (20-24) °C the solid mass fraction of (0.4-1) was obtained.

In [18] the melting process of a salt hydrate PCM was carried out at two different air inlet temperatures (melting temperature +2°C and melting temperature +9°C) and the solid fraction in pouches was determined during melting between (0.62-1).

For this study an **LHTES** consisting of a packed bed of spheres with simple cubic structure, was considered. Each sphere is filled with **PCM**. The advantage that spherical shells have is the high ratio between the outer surface area of the sphere and the interior volume [19].

The goal of the study is to investigate the influence of the air velocity and air inlet temperature on the thermal behaviour of the **LHTES** and on the electrical energy consumption. For this purpose a mathematical model was developed to describe the thermal behaviour of the **LHTES**. The model takes into account the variation of the apparent heat capacity with temperature for the selected **PCM**.

* Corresponding author: mugur.balan@termo.utcluj.ro

2 Material and method

The **LHTES** was designed to reduce the energy consumption of an office building situated in Bucharest, Romania at 44.511° N latitude, 26.078° E longitude and 90 m altitude during the month of July. The climatic data was taken from the Typical Meteorological Year (**TMY**) [20].

The considered office building has two floors, with surface area per floor of 1500 m^2, the height of the total building is 7m and the number of occupants is 180. The specific air flow rate for this type of activity per occupant (25 m^3/h/pers.) and per unit surface area (1.26 m^3/h/pers.) were taken from [21].

2.1. Selection and thermal properties of the PCM

The **PCM** considered for this study was adopted by implementing the selection algorithm, presented in [9], considering the particular climatic conditions of Bucharest, according to the **TMY**. The resulting phase change temperature is in the vicinity of 20°C. Thus the commercially available paraffin **RT20** was chosen [10].

Similar with other paraffin waxes, **RT20** undergoes phase change in a temperature range. Differential scanning calorimetry (**DSC**), is a method that allows the determination of the thermo-physical properties of **PCM**, in small samples. The **DSC** results provide the variation of the heat flux with temperature of the **PCM** during melting and solidification [22], the start (t_s°C) and the end (t_e°C) temperatures of the phase change process, the onset (t_{on}) and the endset (t_{end}) temperatures of the measurement, the peak temperature (t_p°C) where the value of the heat flux assumes a maximal value, and the latent heat for melting and solidification (L [kJ/kg]), which represents the surface area beneath the heat flux curve.

The **DSC** measurements for **RT20** are presented in [12], at three different cooling and heating rates. It is also specified that the cooling and heating rate of the measurement should match the rates of the application, concluding that for a rate of 0.1 K/min the numerical predictions are the most accurate for air conditioning applications [12].

The thermal properties determined in [12] for **RT20**, at a cooling and heating rate of 0.1K/min are presented in table 1.

Table 1 thermal properties of **RT20** at heating and cooling rate of 0.1K/min

Process	t_{on} [°C]	t_s [°C]	t_p [°C]	t_e [°C]	t_{end} [°C]	L [kJ/kg]
Melting	6.8	17.9	21.8	23	23.4	138.3
Solidification	21.8	21.7	21.5	21.1	2.9	143.4

The density of **RT20** is 880 kg/m3 and 770 kg/m3 in solid phase and liquid phase respectively [10].

A thermal hysteresis effect between melting and solidification is observed in the considered **PCM**. The thermal behaviour of the **PCM** during melting and solidification is not identical. There is also a slight difference between the measured latent heat, for solidification and melting. The encapsulation of the **PCM** also contributes to this effect [23]. This effect generates difficulties when estimating the mass fraction of solid and liquid **PCM** as phase change is can be interrupted in free cooling applications. To eliminate the hysteresis effect, for this study, it was assumed that the **PCM** behaves identically during both solidification and melting, considering a theoretical variation of the apparent heat capacity with temperature as a mean value between the apparent heat capacity for solidification and melting. Fig. 1 presents the experimentally determined variation of the apparent heat capacity with temperature for **RT20** and the theoretical mean value considered.

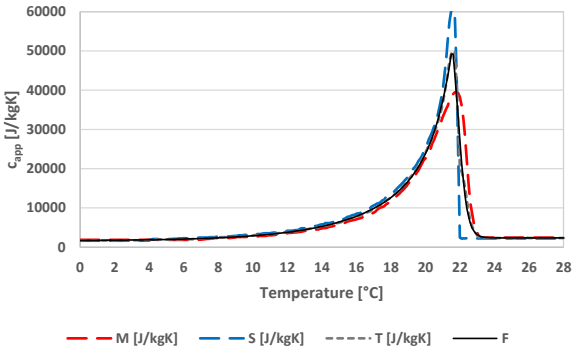

Fig. 1 The apparent heat capacity of **RT20** for melting (M), solidification (S), theoretical mean value (T) and the fitted curve (F)

To take into account the variation of the apparent heat capacity with temperature in the governing thermal balance equations, a curve was fitted that accurately matches the variation. The curve is mathematically described by a discontinuous function as follows:

- An exponential growth of the second order:

$$c_{app,m}(t_{PCM}) = y_0 + A_1 \cdot exp(t_{PCM}/b_1) + A_2 \cdot exp(t_{PCM}/b_2), for\ t_{PCM} < t_p \quad (1)$$

- A Boltzmann variation:

$$c_{app,m}(t_{PCM}) = B_2 + (B_1 - B_2) \cdot \cdot (1 + exp((t_{PCM} - x_0)/d)),\ \ for\ t_{PCM} \geq t_p \quad (2)$$

where $c_{app,m}(t_{PCM})$ is the mean apparent heat capacity as a function of temperature, t_{PCM} is the temperature of the **PCM**. The values of the coefficients A_1, A_2, B_1, B_2, b_1, b_2, d, x_0, y_0, where determined with Origin Lab, and are presented in table 2 and 3.

Table 2 Values of the coefficients -Exp. growth of the second order: $t_{PCM}<t_p$

y_0	A_1	A_2	b_1	b_2
1612.07	4.29E-6	93.27	0.96	3.81

Table 3 Values of the coefficients -Boltzmann variation: $t_{PCM}>t_p$

B_1	B_2	x_0	d
64397.50	2361.30	21.90	0.26

The peak temperature for both solidification and melting was considered to be 21.5°C, and the theoretical latent heat was determined with the following equation:

$$L_{PCM,m} = \int_{t_{on}}^{t_{end}} c_{app,m}(t_{PCM})dt \quad (3)$$

where $L_{PCM,m}$ is the mean latent heat [kJ/kg] for both solidification and melting, assuming a value of 140,50 kJ/kg, determined considering t_{on} and t_{end} at 0°C and 28°C respectively.

2.2 The sizing of the LHTES

A rectangular parallelepiped shape is considered for the **LHTES**, the spheres filled with **RT20** are considered uniformly distributed inside de **LHTES**. The **LHTES** and the characteristic dimensions are presented in fig. 2.

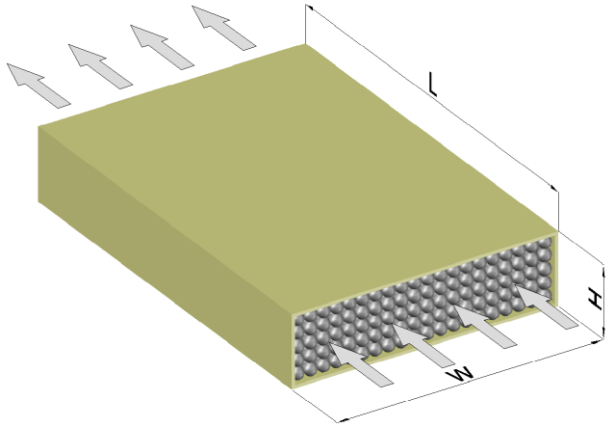

Fig. 2 The **LHTES** and characteristic dimensions

In figure 2, H [m] represents the height, W[m] represents the width and L[m] represents the length of the **LHTES**. The encapsulation material is polyethylene, as in [12].

The **LHTES** was design based on the cooling potential of the exterior air during the nights of July, so to ensure that the mass fraction of the solid **PCM** after the charging period is as high as possible.

The total mass of the **PCM** ($m_{t,PCM}$ [kg]) for the considered **LHTES** was determined as:

$$m_{t,PCM} = \frac{\dot{V}_a \cdot \rho_a \cdot c_a \cdot (t_{s,c} - t_{ext}) \cdot \Delta\tau_h}{L} \quad (4)$$

where $\dot{V}_a$ [m^3/s] is the volumetric air flow rate of the air $\Delta\tau_h$ = 1 hour, ρ_a [kg/m^3] is the density of the air, c_a is the specific heat capacity of the air, t_{ext} [°C] is the exterior air temperature during the night, $t_{s,c}$ [°C] is the temperature at which the solidification starts. For each night of the considered period the total mass of **PCM** was calculated, and an average value was adopted.

2.3 The mathematical model of the LHTES

A mathematical model was developed in order to predict the thermal behavior of the **LHTES**. The governing thermal balance equations are as follows:

$$\dot{m}_a \cdot c_a \cdot \Delta t_a \cdot d\tau = \left[m_{PCM} \cdot c_{app,m}(t_{PCM}) + \rho_s \cdot V_s \cdot c_s\right] \cdot dt_{PCM} \quad (5)$$

$$h \cdot \Delta t_{a,PCM} \cdot S_{PCM} \cdot d\tau = \dot{m}_a \cdot c_a \cdot \Delta t_a \cdot d\tau \quad (6)$$

where $\dot{m}_a$ [kg/s] is the mass air flow rate of the air, t_a [°C] is the exterior air temperature, x [m] is the position of the row of spheres, τ [s] is the time, m_{PCM} is the mass of the **PCM,** h [W/m^2K] is the coefficient of forced convection, ρ_s [kg/m^3] is the density of the encapsulation material, V_s [m^3] is the volume of the encapsulation material, c_s [kJ/kgK] is the specific heat capacity of the encapsulation material, $\Delta t_{a,PCM}$ [°C or K] is the mean logarithmic temperature difference between the air temperature and the **PCM** temperature, and S_{PCM} [m^2] is the heat transfer surface area representing the surface of the **PCM** spheres.

The coefficient of convection was determined as:

$$h = \frac{Nu \cdot \lambda}{d} \quad (7)$$

where Nu [-] is the Nusselt number for forced convection over spheres, calculated with the correlation presented in [24, 25], as follows:

$$Nu = 0.33 \cdot Re^{0.6} \quad (8)$$

where Re [-] is the Reynolds number in the free flowing section.

This correlation is valid for a large range of Re = (20…150000). In the model the variation of the thermo-physical properties of the air, with the temperature, was taken into account.

The following assumptions that are at the basis of the numerical solution are at the basis of the numerical solution:

- It is considered that the mass of all **PCM** spheres on one row is concentrated in one equivalent sphere;
- Spheres are evenly distributed, therefore porosity is constant;
- The temperature of **PCM** spheres from the same row is considered constant;
- Heat transfer through natural convection between the **LHTES** and surrounding environment is neglected;
- The air temperature on the flow section is considered constant

The same assumptions where used in [19].

The mass fraction of the solid **PCM** (γ[-]) was calculated as:

$$\gamma = \frac{\int_{t_{on}}^{t_{PCM}} c_{app,m}(t_{PCM})dt}{\int_{t_{on}}^{t_{end}} c_{app,m}(t_{PCM})dt} \quad (9)$$

2.4 Pressure drop of the LHTES

The local pressure drop of the **LHTES** (Δp [Pa]) was determined:

$$\Delta p = \xi \cdot \frac{\rho_a \cdot w^2}{2} \quad (10)$$

where w [m/s] is the air velocity, ξ is the local pressure drop coefficient of the **LHTES** calculates as [26]:

$$\xi = \frac{1.53}{\varepsilon^{4.2}} \cdot \left(\frac{30}{Re} + \frac{3}{Re^{0.7}} + 0.3 \right) \cdot \frac{L}{d_s} \quad (11)$$

where ε is the porosity of the bed of spheres:

$$\varepsilon = 1 - \frac{\pi}{6 \cdot (1 - \cos\theta \cdot \sqrt{1 + 2 \cdot \cos\theta})} \quad (12)$$

where θ = 90° is the angle of relative placement of the spheres [26] and d_s = 50 mm is the considered exterior diameter of the spheres. The wall thickness of the sphere is 1mm. The considered material from which the spheres were manufactured is polyethylene with a specific heat capacity of c_s=1.55 [kJ/kgK] and a density of ρ_s=925 [kg/m^3] [27].

According to the **TMY**, the ambient air temperatures during the nights of the month of July in Bucharest are ranging from 13°C to 21°C. In order to solidify as much mass as possible the convective heat transfer must be enhanced by increasing the air velocity. This however results in additional energy required for the circulation of air through the **LHTES**. Using the mathematical model, a numerical analysis was carried out, considering a series of constant air inlet (t_i [°C]) temperature in the interval of (13-21) °C, with an increment of 1°C. The air velocity was also increased up to 300%, with a step of 25%, to study both the effect on the heat transfer intensity as well as the impact on the consumed energy.

The electric energy consumed by the fan (E_f [Wh]) was determines as:

$$E_f = \dot{V}_a \cdot \Delta p \cdot \tau / \eta_v \quad (13)$$

where τ [hours] is the operating time and η_v is the efficiency of the fan considered 0.8 for this study.

Each numerical simulation was carried out for a time period of 5h, and the initial **PCM** temperature was considered to be 28°C.

The **LHTES** sizing algorithm was implemented in C++ and the results were exported in Excel.

3 Results and discussions

3.1 The size of the LHTES

The required air flow rate for the considered office building is 8280 m^3/h. The reference air velocity corresponding to this air flow rate is 0.77 m/s. The mass of the **PCM** integrated in the **LHTES** was determined using eq. (4), resulting in a total quantity if 2.065t of **PCM**. The Entire mass of **PCM** was distributed in the **LHTES** rectangular parallelepiped shaped resulting in four heat exchangers with the following dimension: H=0.50 m, W=1.50 m and L=2.20 m.

During cyclic operating conditions, for air cooling application, melting of the entire mass of available **PCM** in the **LHTES** occurs, especially after peak operating conditions. Solidification of the entire mass of **PCM** is however problematic as after peak operating conditions the temperatures of the following night are high. As the mass, heat transfer surface area and size of the **LHTES** are constant parameters, the only method of intensifying the heat transfer between air and **PCM** is by increasing the velocity of the heat transfer fluid, in this case air.

3.2 Influence of air inlet temperature and air velocity

Fig. 3 and 4 present the correlation between the accumulated cold, the mass fractions of solid **PCM** and air velocity, for air inlet temperatures of 13°C, 17°C and 21°C.

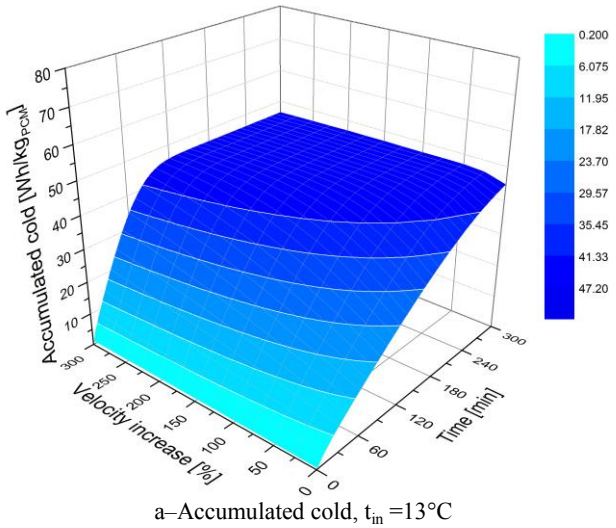

a–Accumulated cold, t_{in} =13°C

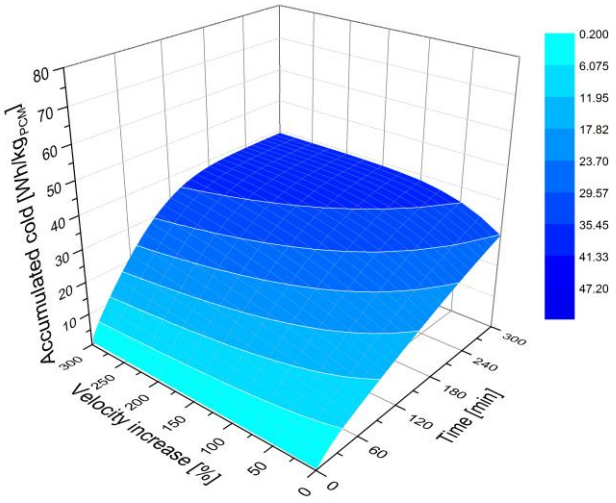

b–Accumulated cold, t_{in} =17°C

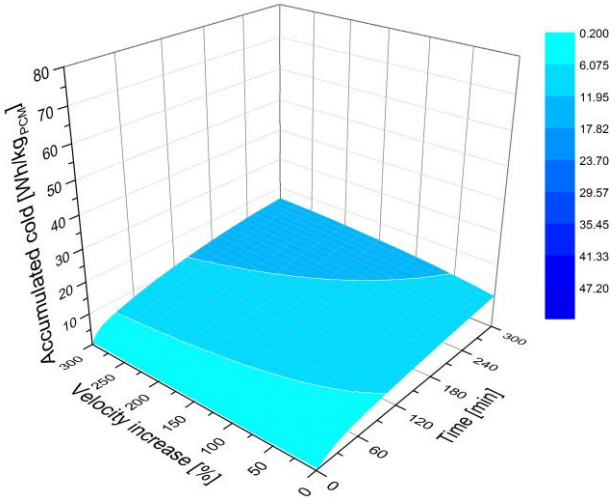

c–Accumulated cold, t_{in} =21°C

Fig. 3 Variation of accumulated cold with air velocity during 5 hours of charging

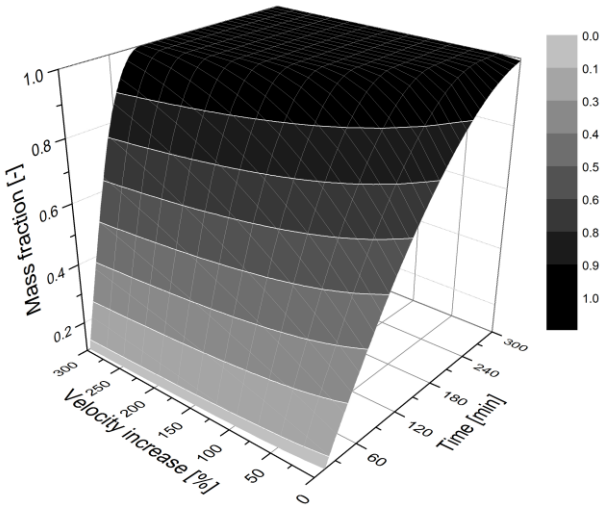

a–Mass fraction of solid **PCM**, t_{in} =13°C

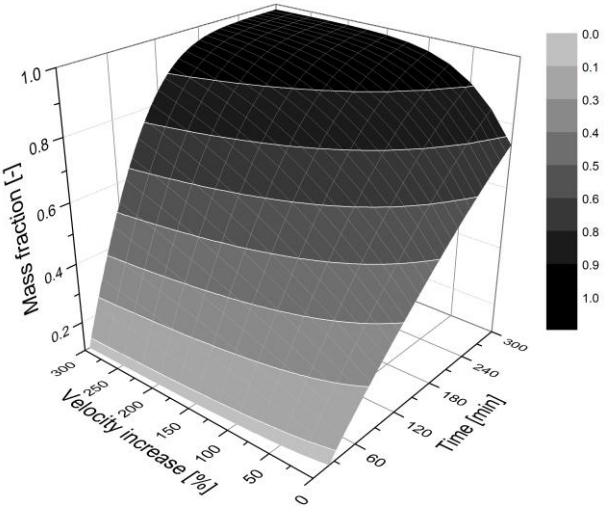

b–Mass fraction of solid **PCM**, t_{in} =17°C

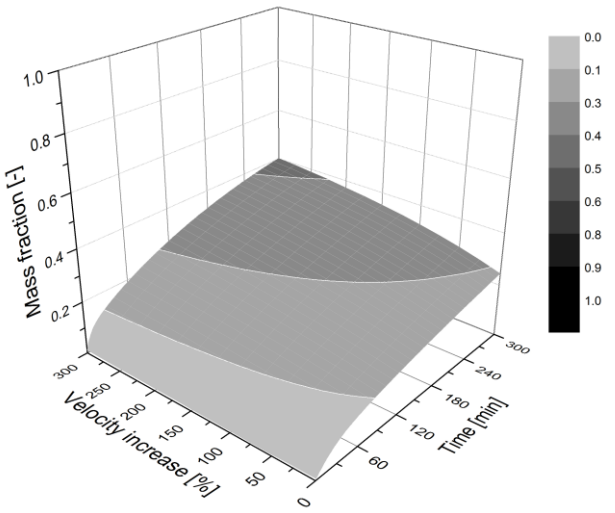

c–Mass fraction of solid **PCM**, t_{in} =21°C

Fig. 4 Variation of mass fraction of the solid **PCM** with air velocity during 5 hours of charging

The influence of air inlet temperature on the electrical energy consumed by the fan is negligible. Considering the air inlet temperature of 13°C as reference, at an air inlet temperature of 21°C the energy consumed by the fan drops with a maximum of only 2.62%. Fig. 5 presents the variation of the accumulated energy consumption of the fan at different velocities during 5h of operation, for an air inlet temperature of 13°C.

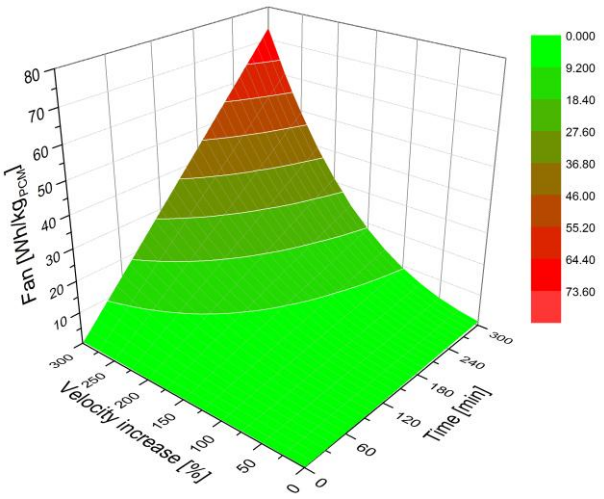

Fig. 5 The variation of electrical Energy absorbed by the Fan with air velocity during 5 hours of charging

Fig. 6 presents the total accumulated cold, at different air velocities and different air inlet temperatures, after five hours of charging. The total accumulated cold [Wh/kg$_{PCM}$] and the electrical energy consumed by the fan [Wh/kg$_{PCM}$] was calculated considering the maximum value of cold that can be stored at the studied air inlet temperature interval, velocities and charging time, as reference.

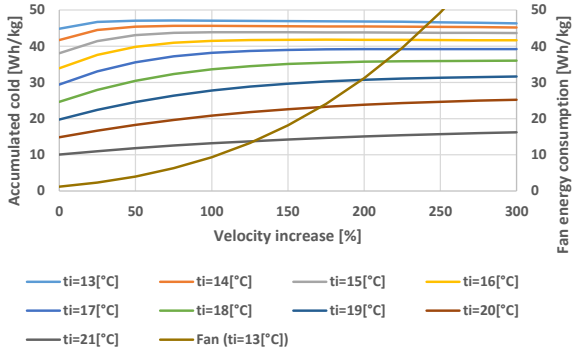

Fig. 6 Variation of accumulated cold and electrical energy consumed by the fan with air velocity, at different air inlet temperatures

The maximum value of cold that can be stored is 47.09 [Wh/kg$_{PCM}$] at an air inlet temperature of 13°C and air velocity of 3.067 m/s. The minimum value of cold that can be stored is 10.06 [Wh/kg$_{PCM}$] at an air inlet temperature of 21°C and at the reference air velocity of 0.77 m/s.

Fig. 7 shows the formation of solid mass of **PCM** at different air velocities and different air inlet temperature, after five hours of charging.

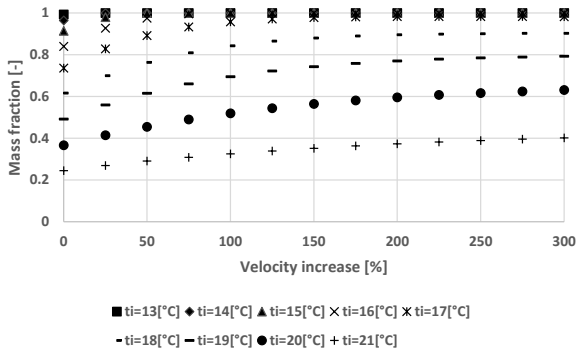

Fig. 7 Evolution of mass fraction of solid **PCM** with air velocity, at different air inlet temperature

A stagnation on the variation curves of accumulated cold and of solid mass fraction of **PCM** is observed in the following cases: for the air temperature of 13 °C, above a velocity increase of 25 %; for the air temperature of (14-15) °C, above a velocity increase of 50 %; for the air temperature of 16 °C, above a velocity increase of 100 %; for the air temperature of 17 °C, above a velocity increase of 150 %.

For air inlet temperature of 18°C the stagnation of the variation of accumulated cold and solid mass fraction of **PCM** is observed at the intersection between the fan's electrical energy consumption curve and the accumulated cold curve. Above this point the fan consumes more energy than the energy stored a cold in the **LHTES**. An air velocity increase of maximum 50% considering the variation of the fan's electrical energy consumption curve is a good compromise between accumulated cold, solidified mass of **PCM** and electrical energy consumption.

For air inlet temperatures between (19-21) °C, for the considered operating conditions, a stagnation zone in this interval is inexistent. An air velocity increase of maximum 50 % considering the variation of the fan's electrical energy consumption curve is a good compromise between accumulated cold, solidified mass of **PCM** and electrical energy consumption.

Table 4 summarizes the variations of the accumulated cold, solid mass formed and energy consumption of the fan, determined by the variations of the inlet air temperature and velocity.

Table 4 Response of the **LHTES** at the variation of the inlet air temperature and velocity

t_i [°C]	↑ w [%]	↑ Q_a [%]	↑ γ [%]	↑ E_{f1} [%]	↑ E_{f2} [%]
13	25	4.20	0.69	92.83	2.50
14	50	8.81	3.63	230.23	6.65
15	50	13.18	9.33	230.19	7.26
16	100	22.36	18.98	673.46	23.78
17	150	32.58	32.83	1399.27	56.79

↑$E_{f1}$is the surplus electric energy consumption of the fan reported to the same value at the reference air velocity
↑$E_{f2}$is the surplus electric energy consumption of the fan reported to the accumulated cold at the reference air velocity
↑Q_a is the increase in accumulated cold

For air inlet temperature of 16°C, the stagnation zone starts at air velocity increase of 100%, where the percentage of energy consumed by the fan and cold stored, when compared to the reference accumulated cold are very close (Q_a=22.36% and E_{f2}=23.78%).

For an air inlet temperature of 17°C, to reach the stagnation zone of the cold accumulation curve at a minimum increase in air velocity of 150%, the electrical energy consumed by the fan increases with 56.79% when compared to the reference accumulated cold, while the cold stored increases with only 32.58% when compared to the reference accumulated cold.

In these cases accumulating the maximum amount of cold at the given parameters requires higher amounts of electrical energy absorbed by the fan.

For the air inlet temperature of 16°C, an increase in air velocity of 75% will lead to 20.80% more cold being accumulated, 18.46% more solid mass being formed while the while the increase in electrical energy consumed by the fan is only 14.86%, when compared to the reference accumulated cold. In this case **PCM** is not fully solidified, the maximum value of the solid mass fraction being 0.995.

The same compromise can be considered for air inlet temperature of 17°C, by reducing the increase in air velocity from 150% to 100%, the resulting increase in accumulated cold is 29.79% with an increase in electrical energy consumption of 27.33%, compared to the reference value, while the maximum value of the solid mass fraction is 0.957. In these cases the stagnation zone of the cold accumulation curve is not reached, however the increase in electrical energy consumption of the **LHTES** is lower than the increase in stored cold.

Fig. 8 and 9 show the **PCM** temperature distribution and mass fraction of solid **PCM** distribution, in the **LHTES** at 17°C and 21°C and the reference air velocity and an air velocity increased by 50%, after five hours of charging.

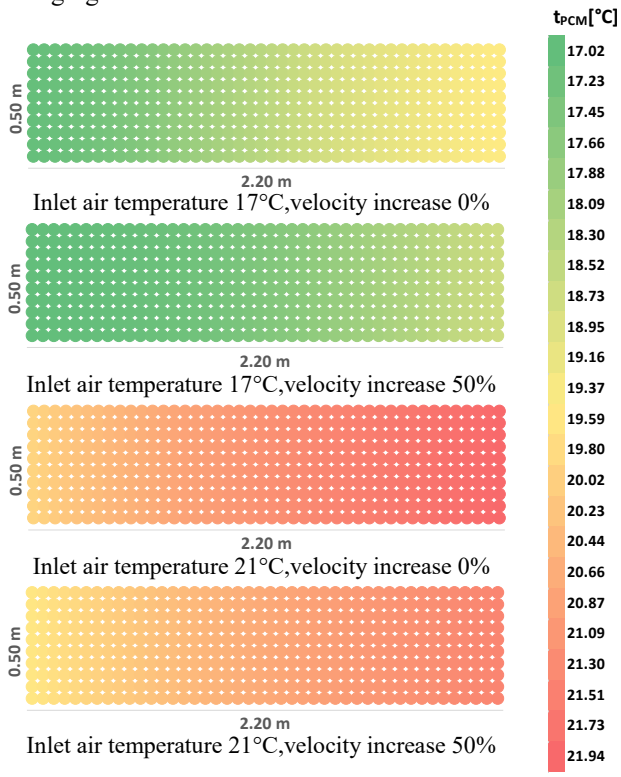

Fig. 8 The **PCM** Temperature distribution in the **LHTES**

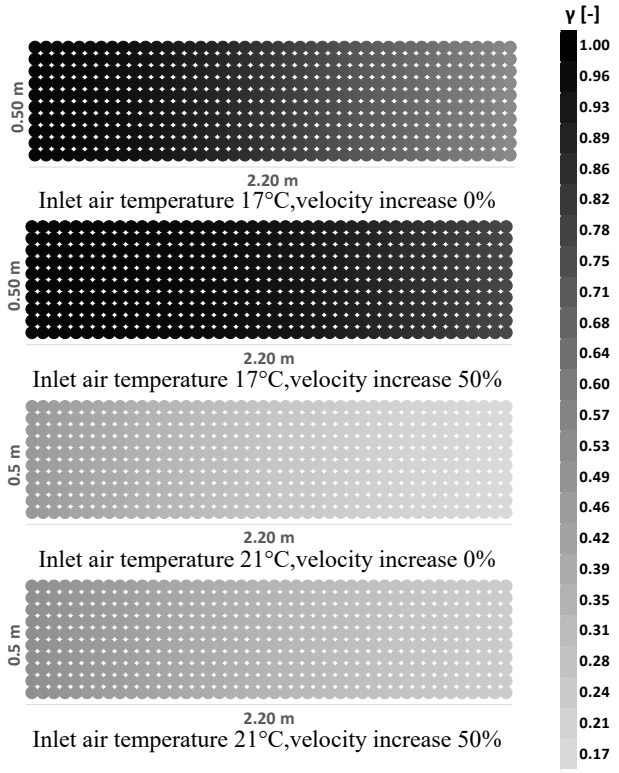

Fig. 9 The mass fraction of solid **PCM** distribution in the **LHTES**

A simulation was carried out (as a case study) for the hottest day of the year in Bucharest, according to the **TMY**, (6th of July), representing the most unfavorable situation for the cold accumulation in the **PCM**. For the air inlet temperatures of (16-19) °C the air velocity and consequently the air flow rate was increased up to 100 % with an increment of 10 %.

Fig. 10 shows the variation of the exterior temperature over a period of 24h according to the **TMY** and end temperature of the solidification process.

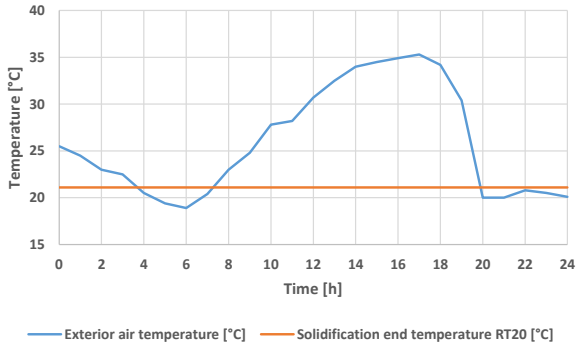

Fig. 10 Variation of the exterior air temperature during the hottest day of July according to the **TMY** and the **PCM** temperature at which solidification ends

As can be seen from fig. 10 the potential for the **PCM** to solidify is limited by the low ambient air temperatures during the charging period, due to the high ambient temperatures. Therefore for air inlet temperatures between (16-19) °C different simulations were carried out where the air velocity was increased up to 100%, with an increment of 10%.

Table 5 presents the influence of air velocity increase during cold accumulation for the hottest day in Bucharest (6th of July) according to the **TMY**.

Table 5 Impact of velocity increase on the accumulated cold (Q_a), and on the corresponding energy absorbed by the fan during cold accumulation (E_f)

↑ **w** [%]	**w** [m/s]	↑**Qa** [%]	↑$\mathbf{E_f}$ [%]
0.0%	0.77	0.00%	0.00%
10.0%	0.84	0.54%	1.23%
20.0%	0.92	1.06%	2.69%
30.0%	1.00	1.58%	4.41%
40.0%	1.07	2.09%	6.42%
50.0%	1.15	2.59%	8.72%
60.0%	1.23	3.09%	11.35%
70.0%	1.30	3.57%	14.32%
80.0%	1.38	4.05%	17.66%
90.0%	1.46	4.56%	21.17%
100.0%	1.53	5.02%	25.30%

It can be observed that by increasing the air velocity up to 100 % when compared to the reference air velocity, the accumulated cod can be increased up to 5.02 % with a supplementary energy consumption of the fan of 25.3 %. These values correspond to an increase of accumulated cold of 59.86 Wh/kg from 57.00 Wh/kg at the reference velocity and an increase of fan energy consumption of 8.89 Wh/kg from 7.10 Wh/kg at the reference velocity.

4 Conclusions

This article presents a numerical analysis of thermal behavior of **LHTES** using **RT20** a commercially available paraffin wax as **PCM**.

The thermal behavior of the **LHTES** was analyzed at different air inlet temperatures and air velocities. The air velocities were increased up to 300% with an increment of 25%. The studied temperature domain was (13-21) °C.

It was observed that at certain values of the air velocity the variation of the cold stored in the **LHTES** stagnate. The stagnation zone starts at an increase in air velocity of: 25% for air inlet temperature of 13°C, 50% for air inlet temperature of 14°C and 15°C, 100% for air inlet temperature of 16°C and 150% for air inlet temperature of 17°C. For the temperature interval of (18-21) °C the stagnation zone is not clearly defined.

The impact on the formation of solid mass of **PCM** and the fan's electrical energy consumption was also investigated.

The numerical investigation identified values of the air velocity where the amount of cold stored in the **LHTES** reaches peak values for certain temperatures.

The study evaluated the favorable impact of the inlet air temperature on the accumulated cold that increase with 346 % from 10.05 Wh/kg at the inlet air temperature of 21 °C to 44.82 Wh/kg at the inlet air temperature of 13 °C, and reference air velocity.

Following the study it was highlighted that a reasonable increase of the air velocity between (25-100) %, depending on air inlet temperatures, determines a benefic impact on the accumulated cold. For the air inlet temperature of 15 °C the amount of accumulated cold solidified mass of **PCM** increases with 13.18% and 9.33% respectively, while the increase in energy consumption of the fan represents 7.26% of the accumulated cold at the reference velocity.

The numerical simulation carried out for the hottest day of July in Bucharest, revealed that the accumulated cold can be increased by 5.02 % with an increase in electrical energy consumption of the fan by 25.30 %. Due to the low air velocities (0.77-1.53) m/s the electrical energy consumed by the fan is relatively low in comparison to the accumulated cold. To store 59.86 Wh/kg of cold in the **LHTES** 8.89 Wh/kg of electrical energy is required, representing 14.91 % energy from the total accumulated cold.

With higher quantities of cold stored in the **LHTES** the operating hours of classic air cooling system can be reduced.

These results must be correlated with the operating hours and energy consumption of chiller which will be the subject of future research activities.

The results presented in this paper were obtained with the support of the Technical University of Cluj-Napoca through the research Contract no. 2013/12.07.2017, Internal Competition CICDI-2017.

References

1. Directive 2010/31/EU of the European Parliament and of the Council of 19 May 2010 on the energy performance of buildings 2010.
2. V.A.A. Raj, R. Velraj, Renewable and Sustainable Energy Reviews, **14**, 2010
3. F.A. Regin, S.C. Solanki, J.S. Saini, Renewable and Sustainable Energy Reviews, **12**, 2008
4. R. Parameshwaran, S. Kalaiselvam, S. Harikrishnan, A. Elayaperumal, Renewable and Sustainable Energy Reviews, **16**, 2012
5. V. Basecq, G. Michaux, C. Inard, P. Blondeau, Advances in Building Energy Research, **7**, 2013
6. E. Osterman, V.V. Tyagi, V. Butala, N.A. Rahim, U.Stritih, Energy and Buildings, **49**, 2012
7. H. Akeiber, P. Nejat, M.Z.A. Majid, M.A. Wahid, F. Jomehzadeh, I.Z. Famileh, J.K. Calautit, B.R. Hughes, S.A. Zaki, Renewable and Sustainable Energy Reviews, **60**, 2016
8. M. Alizadeh, S.M. Sadrameli, Renewable and Sustainable Energy Reviews, **58**, 2016
9. O. Pop, M.C. Balan, Termotehnica, **1** 2016
10. *www.rubitherm.de*
11. *www.pcmproducts.net*
12. C. Arkar, S. Medved, Thermochimica Acta, **438**, 2005
13. M. Iten, S. Liu, A. Shukla, P.D. Silva, Applied Thermal Engineering, **117**, 2017
14. X. Jin, H. Hu, X. Shi, X. Zhang, Energy Conversion and Management, **106**, 2015
15. C. Barreneche, A. Solé, L. Miró, I. Martorell, A.I. Fernández, L.F. Cabeza, Thermochimica Acta, **553** 2013
16. L. Huang, C. Doetsch, C. Pollerberg, International Journal of Refrigeration, **33**, 2010
17. A. Waqas, S. Kumar, Energy and Buildings, **43**, 2011
18. A. Lazaro, P. Dolado, J.M. Marín, B. Zalba, Energy Conversion and Management, **50**, 2009
19. O. Pop, L.F. Tutunaru, M. Balan, Energy Procedia, **112**, 2017
20. MRDPA (Ministry of Regional Development and Public Administration). "Typical meteorological data for Bucharest." (2013) Bucharest, Romania (in Romanian)
21. Normativ pentru proiectarea, executarea si exploatarea instalatiilor de ventilare si climatizare, Indicativ I5. 2010 (in Romanian)
22. A. Hasan, S.J. McCormack, M.J. Huang, B. Norton, Energy Conversion and Management, **81**, 2014
23. K. Kumarasamy, J. An, J. Yang, E.-H. Yang, Energy, **132**, 2017
24. E. Cao, Heat transfer in process engineering, ed. T.M.-H. Companies, 2010
25. N. Leonăchescu, Termotehnică, ed. E.d.ș.p. București, 1981 (in Romanian)
26. I.E. Idelcik, Editura tehnică 1984 (in Romanian)
27. *http://www.firebid.umd.edu/material-database.php*